

# Radial boundary elements method and removing singularity of integrals by an optimal selection of boundary source points

Hossein Hosseinzadeh <sup>\*</sup>, Zeinab Sedaghatjoo

*Department of Mathematics, Persian Gulf University, Bushehr, Iran.*

*July 13, 2023*

## Abstract

Conventionally, piecewise polynomial basis functions (PBFs) are used in the boundary elements method (BEM) to approximate unknown functions. Since, smooth radial basis functions (RBFs) are more stable and accurate than the PBFs for two and three dimensional domains, the unknown functions are approximated by the RBFs in this paper. Therefore, a new formulation of BEM, called radial BEM, is proposed. There are some singular boundary integrals in BEM which mostly are calculated analytically. Analytical schemes are only applicable for PBFs defined on straight boundary element, and become more complicated for polynomials of higher degree. To overcome this difficulty, this paper proposes a distribution for boundary source points so that the boundary integrals can be calculated by Gaussian quadrature rule (GQR) with high precision. Using advantages of the proposed approach, boundary integrals of the radial BEM are calculated, easily and precisely. Several numerical examples are presented to show efficiency of the radial BEM versus standard BEM for solving partial differential equations (PDEs).

**Keywords:** Boundary elements method, Radial basis functions, Singular integrals, Radial BEM.

MSC 2020: 65D12, 65N38, 32A55.

---

<sup>\*</sup>Corresponding author.

*E-mail addresses:*

h.hosseinzadeh@aut.ac.ir , hosseinzadeh@pgu.ac.ir (H. Hosseinzadeh).

z.sedaqatjoo@aut.ac.ir , zeinab.sedaghatjoo@gmail.com (Z. Sedaghatjou).

# 1 Introduction

The Boundary Element Method (BEM) is a numerical method which has been utilized in many branches of science and industry [1, 2, 3, 4]. The main advantage of BEM is transforming a boundary value problem (BVP) to a boundary integral equation (BIE) using Green's identities. BEM reduces computational dimension of the problem by one [5, 6]. This reduction is done by the use of some especial radial functions, called fundamental solutions. Fundamental solutions are unbounded at source points. This unboundedness yields singular boundary integrals which they reduce accuracy of BEM if they are neglected [6, 7]. The integrals can not be evaluated by classical techniques, accurately. Then several techniques have been proposed to deal with this drawback. For instance, analytical techniques [8, 9, 10], semi-analytical techniques [11, 12], exponential transformation techniques [13, 14], distance transformation techniques [15, 16], sinh transformation techniques [17, 18], element subdivision techniques [19, 20, 21] and other innovative techniques [22, 23, 24] are proposed in the literature to overcome this problem. Most of these techniques are restricted to straight boundary elements, Laplace equation and polynomial interpolation. Then obtaining a simple and accurate numerical technique applicable on curved boundary elements, general equation and arbitrary basis functions is still a concerning subject in this area. After analysing the boundary integrals, a new technique is proposed in this paper enjoys these benefits. The new technique is based on finding optimal boundary source points where the (singular and non-singular) boundary integrals are calculated by Gaussian quadrature rule (GQR) with high precision. This is the main novelty of the paper.

The accuracy of the BEM also depends on the approximation power of basis functions defined on the boundary elements. The most common basis functions are polynomials of first, second or higher degree. The BEM obtained by these polynomials are named linear, quadratic and higher order BEM, respectively [6, 12]. These standard basis functions can be replaced by radial basis functions (RBFs). The RBFs are utilized in the literature as an accurate and simple meshless method to solve engineering problems [25, 26, 27, 28]. Since RBFs are more stable than polynomials for data approximation in two and three dimension [29, 21] they are appropriate replacements for polynomials. In [30] RBFs are applied to solve the boundary integral equation arising from Laplace equation with Robin boundary conditions. And in [21] the integral equation is solved by local RBFs. From [30, 21] RBFs lead significantly accurate results when the boundary integrals are calculated, precisely. A new quadrature formula based on the interval sub-division is presented in [31, 32, 33] to compute the integrals. The error analysis presented in the papers show the efficiency of the formula. However the formula is complicated because of splitting the integrals. The RBFs are extended in this paper for solving elliptic equations. Then radial BEM is proposed for which RBFs are applied to estimate boundary values instead of piecewise polynomials. The new method is simple and efficient in application while experiment results show it is significantly more accurate than standard BEM when optimal boundary source points and GQR with  $n = 16$  quadrature nodes are applied.

The rest of the paper is organized as follows. A brief introduction to RBFs and their

implementation for data approximation are presented in Section 2. The radial BEM is described in Section 3 for solving two dimensional PDEs. The singular boundary integrals of BEM are studied in Section 4 and a error analysis is presented there. Then the optimal boundary source points are obtained in Section 5 based on the error analysis. It is shown in the section that GQR with  $n = 16$  nodes is able to calculate the boundary integrals accurately when the optimal boundary source points are applied. Numerical experiments presented in Section 6 verify efficiency of radial BEM versus conventional BEM. Consequently, the paper is completed by a brief conclusion presented in Section 7.

## 2 Radial basis functions

Using RBFs in scattered data approximation was proposed by Hardy [34]. From a point of review, RBFs can be divided into three groups, infinitely smooth, piecewise smooth and compact support RBFs. Some well known RBFs are listed in Table 1. Four first RBFs in this table are infinitely smooth, two RBFs after those are piecewise smooth and two last ones are compactly support [28]. It is well known that infinitely smooth RBFs yield very accurate results when the unknown function is sufficiently smooth [28]. The accuracy of infinitely smooth RBFs mainly depends on the shape parameter,  $\epsilon$ , and the highest accuracy is often obtained at small shape parameters [35, 36].

Table 1: Some RBFs presented in the literature.

list	name	function
1	Gaussian (GA)	$\exp(-\epsilon^2 r^2)$
2	Multiquadric (MQ)	$\sqrt{1 + \epsilon^2 r^2}$
3	Inverse Multiquadric (IMQ)	$1/\sqrt{1 + \epsilon^2 r^2}$
4	Inverse Quadric (IQ)	$1/(1 + \epsilon^2 r^2)$
5	Thin plate spline (TPS)	$r^{2n} \ln(r)$
6	Poly-harmonic Spline (PHS)	$r^{2n+1}$
7	Local $C^0$	$(1 - r)_+^2$
8	Local $C^2$	$(1 - r)_+^4(1 + 4r)$

For numerical approximation by RBFs, let  $(\mathbf{x}_k, b_k)$  are given data for  $k = 1, 2, \dots, K$  where  $\mathbf{x}_k \in \Omega \subseteq \mathbb{R}^2$  and  $b_k \in \mathbb{R}$ . There is a unique function  $q$  satisfying

$$q(\mathbf{x}_k) = b_k, \quad k = 1, 2, \dots, K, \quad (2.1)$$

where

$$q(\mathbf{x}) = \sum_{k=1}^K \gamma_k \phi_k(\mathbf{x}). \quad (2.2)$$

In this equation  $\gamma_k$  is a constant number and  $\phi_k(\mathbf{x}) = \phi(r_k(\mathbf{x}))$  is a RBF where  $r_k(\mathbf{x}) = \|\mathbf{x} - \mathbf{x}_k\|$ . Equation (2.1) can be presented as a system of linear equations

$$\Phi\gamma = \mathbf{b}, \quad (2.3)$$

where

$$\Phi[k, j] = \phi_k(\mathbf{x}_j), \quad \gamma[k] = \gamma_k, \quad \mathbf{b}[k] = b_k, \quad (2.4)$$

for  $k, j = 1, 2, \dots, K$ . The system is non-singular when positive definite RBFs, i.g. Gaussian RBFs, are applied [37, 28, 21], and the interpolation function,  $q$ , admits spectral convergence when infinitely smooth RBFs are utilized [28]. Since Gaussian RBFs are positive definite and infinitely smooth, one can use them to approximate unknown values, safely. Then we mostly use them in this paper.

### 3 Radial BEM

Let  $u$  is a potential function defined on the bounded computational domain,  $\Omega$ , with boundary  $\Gamma$ . The potential function may satisfy partial differential equation

$$\nabla^2 u(\mathbf{x}) + \mathbf{h} \cdot \nabla u(\mathbf{x}) + \lambda u(\mathbf{x}) = 0, \quad (3.1)$$

for  $\mathbf{x} \in \Omega$  where  $\mathbf{h} = [h_1, h_2]$  is a real vector and  $\lambda$  is a constant number. The potential function may also satisfy boundary conditions

$$\begin{cases} u(\mathbf{x}) = \bar{u}(\mathbf{x}), & \text{for } \mathbf{x} \in \Gamma_1, \\ v(\mathbf{x}) = \bar{v}(\mathbf{x}), & \text{for } \mathbf{x} \in \Gamma_2, \end{cases} \quad (3.2)$$

where  $v$  is derivative of  $u$  with respect to  $\mathbf{n}$ , i.e.  $v = \partial u / \partial \mathbf{n}$ , when  $\mathbf{n}$  is outward normal vector defined on the boundary. Also  $\Gamma_1$  and  $\Gamma_2$  are two parts of  $\Gamma$  satisfy  $\Gamma_1 \cup \Gamma_2 = \Gamma$  and  $\Gamma_1 \cap \Gamma_2$  is empty. PDE (3.1) with boundary conditions (3.2) can be transformed to a boundary integral equation. Then, thanks to Divergence theorem and Green's second identity [5, 6], PDE (3.1) is converted to

$$-c(\mathbf{p})u(\mathbf{p}) = \int_{\Gamma} v^*(\mathbf{r})u(\mathbf{q})d\Gamma - \int_{\Gamma} u^*(\mathbf{r})u(\mathbf{q})\mathbf{h} \cdot \mathbf{n} d\Gamma - \int_{\Gamma} u^*(\mathbf{r})v(\mathbf{q})d\Gamma, \quad (3.3)$$

for a source point  $\mathbf{p} \in \mathbb{R}^2$ , field point  $\mathbf{q} \in \Gamma$  and  $\mathbf{r} = \mathbf{q} - \mathbf{p}$ . New parameters  $\mathbf{p}$ ,  $\mathbf{q}$  and  $\mathbf{r}$  are shown in Figure 1, graphically. In BIE (3.3) we have  $c(\mathbf{p}) = \alpha/2\pi$  where  $\alpha$  is interior angle respect to the source point  $\mathbf{p}$  [6]. It is well-known that  $c(\mathbf{p}) = 1$  when  $\mathbf{p}$  is in  $\Omega$ , it equals 0.5 when  $\mathbf{p}$  is located at smooth part of the boundary and it vanishes when  $\mathbf{p}$  is out of the region. Function  $u^*$  is fundamental solution of the PDE and  $v^* = \partial u^* / \partial \mathbf{n}$ . The main advantage of the fundamental solution is that it satisfies

$$\nabla^2 u^*(\mathbf{r}) - \mathbf{h} \cdot \nabla u^*(\mathbf{r}) + \lambda u^*(\mathbf{r}) = -\delta(\mathbf{r}),$$

where  $\delta$  is Dirac delta function [6, 38] satisfies  $\delta(\mathbf{r}) = \infty$  for  $\mathbf{r} = (0, 0)$  and  $\delta(\mathbf{r}) = 0$ , elsewhere. Fundamental solutions of PDEs are reported in [6, 38, 39].

To solve integral equation (3.3), field points  $\mathbf{q}_1, \mathbf{q}_2, \dots, \mathbf{q}_N, \mathbf{q}_{N+1}$  are selected on the boundary of computational domain anticlockwise such that the last point overlaps with the first point, i.e.  $\mathbf{q}_1 = \mathbf{q}_{N+1}$ . Then geometry of the boundary is approximated by  $N$  boundary elements obtained by connecting the field points, successively. After that, boundary values over the elements are approximated by some basis functions. Conventionally, polynomials of order less than or equal to 2 are applied for the approximation [12, 6]. Consequently, BIE (3.3) is simplified to

$$\begin{aligned} -c(\mathbf{p})u(\mathbf{p}) &= \sum_{j=1:N} \frac{l_j}{2} \int_{-1}^1 v^*(\mathbf{r}_j(t))u(q_j(t))dt \\ &\quad - \sum_{j=1:N} \frac{l_j}{2} \mathbf{h} \cdot \mathbf{n}_j \int_{-1}^1 u^*(\mathbf{r}_j(t))u(q_j(t))dt \\ &\quad - \sum_{j=1:N} \frac{l_j}{2} \int_{-1}^1 u^*(\mathbf{r}_j(t))v(q_j(t))dt, \end{aligned} \quad (3.4)$$

where  $l_j$  is length of  $j$ -th boundary element,  $\Gamma_j$ , i.e.  $l_j = \|\mathbf{q}_{j+1} - \mathbf{q}_j\|$ . And  $\mathbf{r}_j(t) = q_j(t) - \mathbf{p}$  where  $q_j$  is a linear function varies from  $\mathbf{q}_j$  to  $\mathbf{q}_{j+1}$  when  $t$  varies from  $-1$  to  $1$ , i.e.

$$q_j(t) = \frac{\mathbf{q}_{j+1} + \mathbf{q}_j}{2} + \frac{\mathbf{q}_{j+1} - \mathbf{q}_j}{2}t, \quad t \in [-1, 1]. \quad (3.5)$$

Besides,  $\mathbf{n}_j$  is outward normal vector perpendicular to boundary element  $\Gamma_j$ . See Figure 1 for more understanding. Note that, linear approximation (3.5) leads simplified equation (3.4) by assuming straight boundary elements. However one can omit the linear approximation and assume more complicated curved boundary elements. In Figure 6 the boundary elements are assumed straight and curved for square and flower-like domains, respectively.

Generally, there are two kinds of boundary integrals in Eq. (3.4) which have to be obtained. They are

$$I_1 = \int_{-1}^1 v^*(\mathbf{r}_j(t))g(t)dt, \quad I_2 = \int_{-1}^1 u^*(\mathbf{r}_j(t))g(t)dt, \quad (3.6)$$

where  $g(t)$  is a smooth function defined on interval  $[-1, 1]$ . Fundamental solution  $u^*$  and its derivative respect to  $\mathbf{n}$ ,  $v^*$ , may be unbounded at  $\mathbf{r}_j = (0, 0)$ , so conventional numerical methods, such as standard Gaussian quadrature rule, are not able to calculate the boundary integrals accurately. Then, we should use some special tools to calculate these boundary integrals when source point  $\mathbf{p}$  is located at the boundary element  $\Gamma_j$ . A new approach is proposed in section 5 where it enables us to calculate the integrals accurately by the Gaussian quadrature rule. In the Gaussian quadrature rule,  $n$  quadrature nodes are selected on each boundary element and an integral over the boundary element is approximated by a weighted summation [6]. If the union of the quadrature nodes and weights

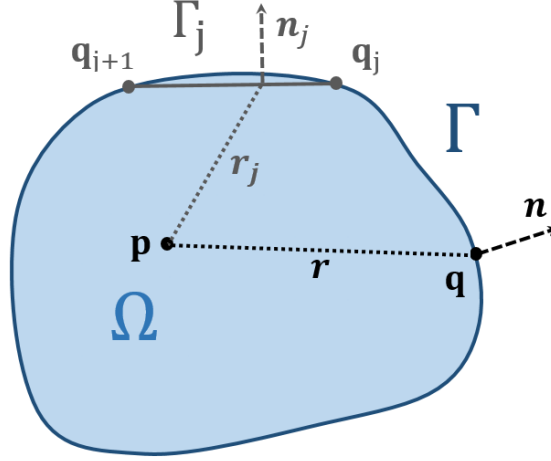


Figure 1: Computational domain  $\Omega$  and its boundary,  $\Gamma$ . Source point,  $\mathbf{p}$ , field point,  $\mathbf{q}$ , and distance vector,  $\mathbf{r}$  are shown in this picture. Also, one can see field points  $\mathbf{q}_{j+1}$  and  $\mathbf{q}_j$  are connected to each other by straight boundary element  $\Gamma_j$ .

defined on the boundary elements are inserted in two vectors  $\mathbf{q}_G$  and  $\mathbf{w}_G$ , respectively, then

$$\int_{\Gamma} f(\mathbf{q}) d\Gamma \simeq \sum_{j=1:N} \int_{\Gamma_j} f(\mathbf{q}) d\Gamma_j \simeq \sum_{s=1:nN} f(\mathbf{q}_G[s]) \mathbf{w}_G[s] = f(\mathbf{q}_G) \mathbf{w}_G^T, \quad (3.7)$$

for a real function  $f$ . In this approximation,  $f(\mathbf{q}_G)$  is the value of  $f$  at  $\mathbf{q}_G$ . Since vectors  $\mathbf{q}_G$  and  $\mathbf{w}_G$  are utilized frequently in this paper, we call them quadrature nodes and weights, respectively, here after.

Now, let  $\phi_1, \phi_2, \dots, \phi_K$  are some basis functions defined on  $\Gamma$ . Then boundary functions  $u$  and  $v$  may be approximated by these basis functions as

$$u(\mathbf{q}) = \sum_{k=1:K} \alpha_k \phi_k(\mathbf{q}), \quad v(\mathbf{q}) = \sum_{k=1:K} \beta_k \phi_k(\mathbf{q}), \quad (3.8)$$

for each field point  $\mathbf{q} \in \Gamma$ . In special case, the basis functions can be radial, i.e.

$$\phi_k(\mathbf{q}) = \phi(\|\mathbf{q} - \mathbf{p}_k\|), \quad k = 1, 2, \dots, K,$$

when  $\mathbf{p}_1, \mathbf{p}_2, \dots, \mathbf{p}_K$  are  $K$  different center points located on  $\Gamma$ . Note that equations in (3.8) can be write in vector form

$$u(\mathbf{q}) = \boldsymbol{\phi}(\mathbf{q}) \boldsymbol{\alpha}^T, \quad v(\mathbf{q}) = \boldsymbol{\phi}(\mathbf{q}) \boldsymbol{\beta}^T, \quad (3.9)$$

where  $\boldsymbol{\alpha} = [\alpha_1, \alpha_2, \dots, \alpha_K]$ ,  $\boldsymbol{\beta} = [\beta_1, \beta_2, \dots, \beta_K]$  and  $\boldsymbol{\phi}(\mathbf{q}) = [\phi_1(\mathbf{q}), \phi_2(\mathbf{q}), \dots, \phi_K(\mathbf{q})]$ . This vector form helps us to express coefficient vectors  $\boldsymbol{\alpha}$  and  $\boldsymbol{\beta}$  as functions of  $u$  and  $v$ , respectively when it is necessary. By inserting equations (3.8) in boundary integral equation

(3.4) we have

$$\begin{aligned}
-c(\mathbf{p}) \sum_{k=1:K} \alpha_k \phi_k(\mathbf{p}) &= \sum_{k=1:K} \alpha_k \sum_{j=1:N} \frac{l_j}{2} \int_{-1}^1 v^*(\mathbf{r}_j(t)) \phi_k(q_j(t)) dt \\
&- \sum_{k=1:K} \alpha_k \sum_{j=1:N} \frac{l_j}{2} \mathbf{h} \cdot \mathbf{n}_j \int_{-1}^1 u^*(\mathbf{r}_j(t)) \phi_k(q_j(t)) dt \\
&- \sum_{k=1:K} \beta_k \sum_{j=1:N} \frac{l_j}{2} \int_{-1}^1 u^*(\mathbf{r}_j(t)) \phi_k(q_j(t)) dt,
\end{aligned} \tag{3.10}$$

where one dimensional boundary integrals can be calculated numerically by the Gaussian quadrature rule as Equation (3.7) when boundary source points are optimal. Finding the optimal center points is the main subject of Section 5 and we only focus on obtaining the final system of linear equations of the new formulation in this section. Then, let boundary integrals in Equation (3.10) are calculated by Equation (3.7), accurately. In this situation, Equation (3.10) can be write in matrix form

$$-c(\mathbf{p}) \phi(\mathbf{p}) \boldsymbol{\alpha}^T = \mathbf{H}_\mathbf{p} \boldsymbol{\Phi} \boldsymbol{\alpha}^T - \mathbf{G}_\mathbf{p}^1 \boldsymbol{\Phi} \boldsymbol{\alpha}^T - \mathbf{G}_\mathbf{p}^2 \boldsymbol{\Phi} \boldsymbol{\beta}^T, \tag{3.11}$$

where vectors  $\mathbf{H}_\mathbf{p}$ ,  $\mathbf{G}_\mathbf{p}^1$ ,  $\mathbf{G}_\mathbf{p}^2$  and matrix  $\boldsymbol{\Phi}$  are evaluated as

$$\begin{aligned}
\mathbf{H}_\mathbf{p} &= v^*(\mathbf{q}_G - \mathbf{p}) \cdot * \mathbf{w}_G, \\
\mathbf{G}_\mathbf{p}^1 &= u^*(\mathbf{q}_G - \mathbf{p}) \cdot * (\mathbf{h} \cdot \mathbf{n}(\mathbf{q}_G)) \cdot * \mathbf{w}_G, \\
\mathbf{G}_\mathbf{p}^2 &= u^*(\mathbf{q}_G - \mathbf{p}) \cdot * \mathbf{w}_G, \\
\boldsymbol{\Phi}[:, k] &= \phi_k(\mathbf{q}_G),
\end{aligned} \tag{3.12}$$

The notation  $*$  shows Hadamard (or dot) product. For two matrices  $A$  and  $B$  of the same size, Hadamard product  $A * B$  is a matrix which is evaluated as

$$(A * B)[i, j] = A[i, j] B[i, j].$$

It should be mentioned that  $\mathbf{n}(\mathbf{q}_G)$  which is presented in  $\mathbf{G}_\mathbf{p}^1$  is a matrix with two rows. The first and second rows of  $\mathbf{n}(\mathbf{q}_G)$  are devoted to the first and second components of normal vector  $\mathbf{n}$  at quadrature nodes  $\mathbf{q}_G$ , respectively. And  $\boldsymbol{\Phi}[:, k]$  denotes  $k$ -th column of matrix  $\boldsymbol{\Phi}$ .

To find unknown vectors  $\boldsymbol{\alpha}$  and  $\boldsymbol{\beta}$  we need  $2K$  equations. The first  $K$  equations are obtained by inserting boundary source points  $\mathbf{p}_1, \mathbf{p}_2, \dots, \mathbf{p}_K$  in Equation (3.11) instead of  $\mathbf{p}$ , and the last  $K$  equations are obtained via boundary conditions (3.2). By inserting the boundary source points in Equation (3.11), system of linear equations

$$-\frac{1}{2} \boldsymbol{\Phi} \boldsymbol{\alpha}^T = \mathbf{H} \boldsymbol{\Phi} \boldsymbol{\alpha}^T - \mathbf{G}^1 \boldsymbol{\Phi} \boldsymbol{\alpha}^T - \mathbf{G}^2 \boldsymbol{\Phi} \boldsymbol{\beta}^T, \tag{3.13}$$

is obtained where  $k$ -th row of matrices  $\boldsymbol{\Psi}$ ,  $\mathbf{H}$ ,  $\mathbf{G}^1$  and  $\mathbf{G}^2$  are evaluated as

$$\begin{aligned}
\boldsymbol{\Psi}[k, :] &= \phi(\mathbf{p}_k), & \mathbf{H}[k, :] &= \mathbf{H}_{\mathbf{p}_k}, \\
\mathbf{G}^1[k, :] &= \mathbf{G}_{\mathbf{p}_k}^1, & \mathbf{G}^2[k, :] &= \mathbf{G}_{\mathbf{p}_k}^2.
\end{aligned}$$

Equation (3.13) can be simplified to matrix form

$$\mathbf{A}\boldsymbol{\alpha}^T = \mathbf{B}\boldsymbol{\beta}^T, \quad (3.14)$$

where

$$\mathbf{A} = \frac{1}{2}\boldsymbol{\Phi} + \mathbf{H}\boldsymbol{\Phi} - \mathbf{G}^1\boldsymbol{\Phi} \quad , \quad \mathbf{B} = \mathbf{G}^2\boldsymbol{\Phi}.$$

If we define vectors

$$\begin{aligned} \mathbf{u} &= [u(\mathbf{p}_1), u(\mathbf{p}_2), \dots, u(\mathbf{p}_K)], \\ \mathbf{v} &= [v(\mathbf{p}_1), v(\mathbf{p}_2), \dots, v(\mathbf{p}_K)], \end{aligned} \quad (3.15)$$

then Equation (3.9) leads

$$\mathbf{u}^T = \boldsymbol{\Psi}\boldsymbol{\alpha}^T, \quad \mathbf{v}^T = \boldsymbol{\Psi}\boldsymbol{\beta}^T. \quad (3.16)$$

From boundary conditions (3.2), functions  $u$  and  $v$  is equal to  $\bar{u}$  and  $\bar{v}$  on  $\Gamma_1$  and  $\Gamma_2$ , respectively. So if we suppose boundary points  $\{\mathbf{p}_1, \mathbf{p}_2, \dots, \mathbf{p}_{K_1}\}$  and  $\{\mathbf{p}_{K_1+1}, \mathbf{p}_{K_1+2}, \dots, \mathbf{p}_K\}$  are located on  $\Gamma_1$  and  $\Gamma_2$ , respectively, the boundary conditions can be imposed as

$$\begin{cases} \mathbf{u}[k] = \bar{u}(\mathbf{p}_k), & \text{for } k = 1, 2, \dots, K_1, \\ \mathbf{v}[k] = \bar{v}(\mathbf{p}_k), & \text{for } k = K_1 + 1, K_1 + 2, \dots, K. \end{cases} \quad (3.17)$$

Now equations (3.14), (3.16) and (3.17) lead the final system of linear equations

$$\begin{bmatrix} \mathbf{A} & -\mathbf{B} & \mathbf{0} & \mathbf{0} \\ \boldsymbol{\Psi} & \mathbf{0} & -\mathbf{I} & \mathbf{0} \\ \mathbf{0} & \boldsymbol{\Psi} & \mathbf{0} & -\mathbf{I} \\ \mathbf{0} & \mathbf{0} & \mathbf{C}_1 & \mathbf{C}_2 \end{bmatrix} \begin{bmatrix} \boldsymbol{\alpha}^T \\ \boldsymbol{\beta}^T \\ \mathbf{u}^T \\ \mathbf{v}^T \end{bmatrix} = \begin{bmatrix} \mathbf{0}^T \\ \mathbf{0}^T \\ \mathbf{0}^T \\ \bar{\mathbf{w}}^T \end{bmatrix}, \quad (3.18)$$

where  $\mathbf{0}$  and  $\mathbf{0}^T$  are zero matrix and vector, respectively, and  $\mathbf{I}$  is the identity matrix. Also matrices  $\mathbf{C}_1$  and  $\mathbf{C}_2$  and vector  $\bar{\mathbf{w}}$  are defined to impose the boundary conditions which are evaluated as  $\mathbf{C}_1[k, k] = 1$  for  $k = 1, 2, \dots, K_1$  and 0 otherwise,  $\mathbf{C}_2[k, k] = 1$  for  $k = K_1 + 1, K_1 + 2, \dots, K$  and 0 otherwise,  $\bar{\mathbf{w}}[k] = \bar{u}(\mathbf{p}_k)$  for  $k = 1, 2, \dots, K_1$  and  $\bar{\mathbf{w}}[k] = \bar{v}(\mathbf{p}_k)$  for  $k = K_1 + 1, K_1 + 2, \dots, K$ .

After solving the final system and obtaining vectors  $\boldsymbol{\alpha}$ ,  $\boldsymbol{\beta}$ ,  $\mathbf{u}$  and  $\mathbf{v}$ , the potential function  $u$  can be calculated at an internal point  $\mathbf{p} \in \Omega$  as

$$u(\mathbf{p}) = -\mathbf{H}_{\mathbf{p}}\boldsymbol{\Phi}\boldsymbol{\alpha}^T + \mathbf{G}_{\mathbf{p}}^1\boldsymbol{\Phi}\boldsymbol{\alpha}^T + \mathbf{G}_{\mathbf{p}}^2\boldsymbol{\Phi}\boldsymbol{\beta}^T, \quad (3.19)$$

by Equation (3.11) where matrices  $\mathbf{H}_{\mathbf{p}}$ ,  $\boldsymbol{\Phi}$ ,  $\boldsymbol{\Phi}_{\mathbf{n}}$ ,  $\mathbf{G}_{\mathbf{p}}^1$  and  $\mathbf{G}_{\mathbf{p}}^2$  are defined in Equation (3.12).

## 4 Error analysis of the Gaussian quadrature rule

Let Gaussian quadrature rule (GQR) with  $n$  quadrature nodes is applied to calculate the boundary integrals defined on each  $\Gamma_j$  for  $j = 1, 2, \dots, N$ . Therefore,  $n \times N$  boundary nodes are selected on the boundary where they are inserted in a vector, named quadrature points



and denoted by  $\mathbf{q}_G$ . The weights respect to these points are also inserted in a vector. The vector is named quadrature weights and denoted by  $\mathbf{w}_G$ . Then, these vectors are applied to approximate the boundary integral as Equation (3.7). Note that the numerical integration (3.7) is only valid for smooth functions, and it does not lead accurate result when  $f$  is not continuous. Unfortunately, integrals of BEM are singular at source points and the rule loses its efficiency for them. In this section we show the singular integrals also can be estimated by the rule, accurately if the boundary source points are selected appropriately. Therefore, a numerical technique is proposed here to find optimal boundary source points  $\mathbf{p}_1, \mathbf{p}_2, \dots, \mathbf{p}_K$  such that Approximation (3.7) is accurate for integrals (3.6).

Since accuracy of GQR may be reduced when  $\mathbf{p}_k = q_j(s)$  for some  $s \in [-1, 1]$ , we look for the optimal value of  $s$  satisfies

$$I_1 = \int_{-1}^1 v^*(q_j(t) - q_j(s)) g(t) dt \simeq \sum_{i=1:n} v^*(q_j(t_i) - q_j(s)) g(t_i) w_i, \quad (4.1)$$

$$I_2 = \int_{-1}^1 u^*(q_j(t) - q_j(s)) g(t) dt \simeq \sum_{i=1:n} u^*(q_j(t_i) - q_j(s)) g(t_i) w_i, \quad (4.2)$$

where  $t_1, t_2, \dots, t_n$  and  $w_1, w_2, \dots, w_n$  are the standard Gaussian quadrature nodes and weights, respectively [40]. It will be shown in continue that the optimal value does not significantly depend on functions  $v^*, u^*$  and  $g$ , but it mainly depends on the number of Gaussian nodes, i.e.  $n$ . Note that integrand function in Equation (4.1), is vanished at  $s = t$  while it is unbounded when  $t$  tends to  $s$  [6]. Then integral Approximation (4.2) is the main concerning problem studied in this section. Error of approximation (4.2) is studied here and the optimal value of  $s$  minimises the error is obtained in the next section.

The fundamental solutions of Helmholtz and advection-diffusion equations have the modified Bessel function,  $K_0(\|\mathbf{r}\|)$ , in their formulations [6, 38, 39]. Since

$$K_0(\|\mathbf{r}\|) \simeq -\ln(\|\mathbf{r}\|) + \ln(2) - 0.5772, \quad (4.3)$$

when  $\|\mathbf{r}\|$  tends to zero, it can be found the fundamental solution is not bounded at  $\mathbf{r} = (0, 0)$  [5]. Semi-equality (4.3) also highlights magnitude of the fundamental solution increases as rate as  $-\ln(\|\mathbf{r}\|)$  when  $\|\mathbf{r}\|$  tends to zero. Then semi-equality (4.2) will be accurate if and only if semi-equality

$$\int_{-1}^1 \ln(\|q_j(t) - q_j(s)\|) g(t) dt \simeq \sum_{i=1:n} \ln(\|q_j(t_k) - q_j(s)\|) g(t_k) w_k, \quad (4.4)$$

is accurate. From Equation (3.5),  $q_j(t) = q_j(s)$  if  $t = s$  then approximation (4.4) will be accurate if semi-equality

$$\int_{-1}^1 \ln(\|t - s\|) g(t) dt \simeq \sum_{k=1:n} \ln(\|t_k - s\|) g(t_k) w_k, \quad (4.5)$$

is accurate. Then in mathematical sense, we are looking for that  $s$  minimises the error function

$$Err(s) = \left| \int_{-1}^1 \ln(\|t - s\|) g(t) dt - \sum_{k=1:n} \ln(\|t_k - s\|) g(t_k) w_k \right|. \quad (4.6)$$

Note that the error function mainly depends on number of Gaussian nodes,  $n$ . It also depends on smooth function  $g$ . To omit the rule of  $g$ , the function is expanded around  $s$  by Taylor's expansion formula as

$$g(t) = \sum_{i=0:\infty} g^{(i)}(s) (t - s)^i / i! \simeq g(s) + g'(s) (t - s) + g''(s) (t - s)^2 / 2,$$

where by inserting the expansion in the error function (4.6) we have

$$Err(s) \leq \sum_{i=0:\infty} |g^{(i)}(s)| Err^i(s) / i! \simeq |g(s)| Err^0(s) + |g'(s)| Err^1(s) + |g''(s)| Err^2(s) / 2,$$

when

$$Err^i(s) = \left| \int_{-1}^1 \ln(\|t - s\|) \|t - s\|^i dt - \sum_{k=1:n} \ln(\|t_k - s\|) \|t_k - s\|^i w_k \right|. \quad (4.7)$$

From Equation (4.7), one can find that  $Err^i$  is error of numerical integration of function  $f^i(r) = \ln(r)r^i$  from  $-1$  to  $1$  when  $r = \|t - s\|$ . We know  $f^0(r)$  is unbounded at  $r = 0$  while  $f^1(r)$  is continuous and  $f^i(r)$  is differentiable at this point for  $i \geq 2$ . Since the Gaussian quadrature rule is more accurate for smoother functions, it seems the error of the rule decreases when  $i$  increases. Graph of  $Err^0$ ,  $Err^1$  and  $Err^2$  are shown in Figure 2 for  $n = 8$  and  $16$  and  $s \in [0, 1]$ . Since  $Err^i$  is symmetric with respect to  $s$ , then  $Err^i(s) = Err^i(-s)$  for  $s < 0$ . The figure verifies  $Err^0 \leq Err^1 \leq Err^2$  almost everywhere. Therefore  $Err^0$  is the main part of the error function,  $Err$ , and

$$Err(s) \simeq |g(s)| Err^0(s). \quad (4.8)$$

## 5 Optimal boundary source points

Now we are going to find the optimal value of  $s$  minimizes the error function, i.e.

$$s_{opt} = \arg \min_{s \in [-1, 1]} Err(s). \quad (5.1)$$

Thanks to semi-equality (4.8), the error function gets its minimum nearly at zeros of  $Err^0$  because  $Err^i(s) \leq Err^0(s)$  almost everywhere for  $i \geq 1$ . Consequently, the optimal value also satisfies

$$s_{opt} \simeq \arg \min_{s \in [-1, 1]} Err^0(s). \quad (5.2)$$

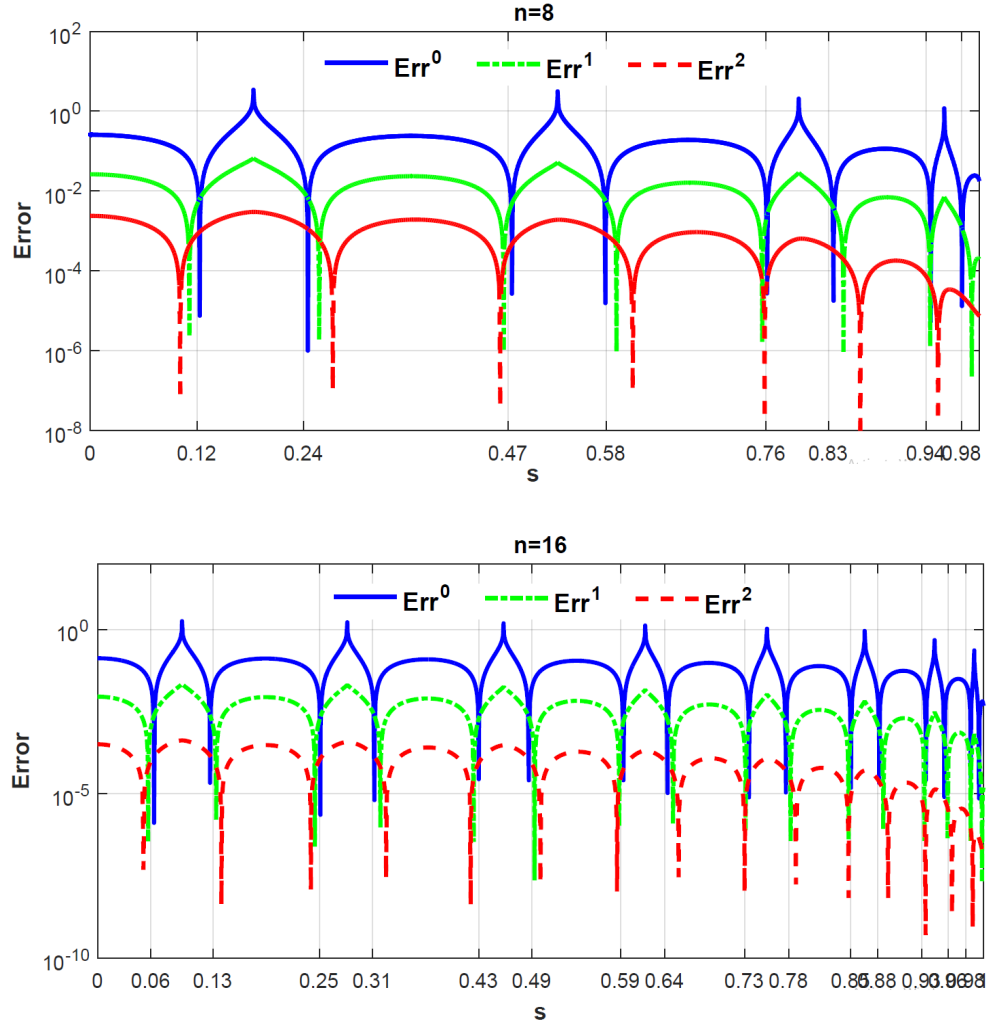


Figure 2: Graph of  $Err^0$ ,  $Err^1$  and  $Err^2$  in field of  $s \in [0, 1]$ . Number of Gaussian quadrature nodes is  $n = 8$  and 16 for upper and lower pictures, respectively. We see  $Err^2 \leq Err^1 \leq Err^0(s)$  almost everywhere. Also in this figure  $Err^0(s)$  is vanished at  $s = 0.12, 0.24, 0.47, 0.58, 0.76, 0.83, 0.94, 0.98$  and  $s = 0.06, 0.13, 0.25, 0.31, 0.43, 0.49, 0.59, 0.64, 0.73, 0.78, 0.85, 0.88, 0.93, 0.96, 0.98$  for  $n = 8$  and 16, respectively.

In Figure 2 graph of  $Err^0$  is depicted for  $n = 8$  and 16 and  $s \in [0, 1]$ . From Figure 2 and this fact that  $Err^0(s)$  is symmetric with respect to  $s$ , the zeros of  $Err^0$  can be reported as

$$s = \begin{cases} \begin{cases} \pm 0.12, \pm 0.24, \pm 0.47, \pm 0.58, \\ \pm 0.76, \pm 0.83, \pm 0.94, \pm 0.98, \end{cases} & \text{if } n = 8, \\ \begin{cases} \pm 0.06, \pm 0.13, \pm 0.25, \pm 0.31, \pm 0.43, \pm 0.49, \pm 0.59, \\ \pm 0.64, \pm 0.73, \pm 0.85, \pm 0.88, \pm 0.93, \pm 0.96, \pm 0.98, \end{cases} & \text{if } n = 16. \end{cases} \quad (5.3)$$

These points satisfy Equation (5.2) and they are appropriate candidates for  $s_{opt}$ . Then efficiency of these points are checked by some numerical experiments in continue.

**Example 5.1.** Let  $\Omega = [-1, 1]^2$  and its boundary,  $\Gamma$ , is discretized to  $N$  equal boundary elements. Then,  $K = 2N$  source points

$$\{\mathbf{p}_1, \mathbf{p}_2\}, \{\mathbf{p}_3, \mathbf{p}_4\}, \dots, \{\mathbf{p}_{2N-1}, \mathbf{p}_{2N}\}, \quad (5.4)$$

are selected on the boundary elements where couples  $\{\mathbf{p}_{2j-1}, \mathbf{p}_{2j}\}$  are selected on  $j$ -th boundary element,  $\Gamma_j$ , such that  $\mathbf{p}_{2j-1} = q_j(-s)$  and  $\mathbf{p}_{2j} = q_j(s)$  for an  $s \in [-1, 1]$ . The Laplace equation

$$\nabla^2 u(x, y) = 0, \quad (x, y) \in \Omega, \quad (5.5)$$

with Dirichlet boundary condition  $u = \bar{u}$  is imposed on the boundary source points, and the linear BEM is applied to obtain the flux function,  $v$ , at the boundary points. Two exact solutions

$$\text{Eq. 1: } u(x, y) = x^2 - y^2, \quad (5.6)$$

$$\text{Eq. 2: } u(x, y) = \exp(x) \cos(y). \quad (5.7)$$

are considered here to study the accuracy of the BEM. Boundary integrals of the method are calculated by GQR with  $n$  quadrature nodes, and error of the method is calculated by error function

$$Er(s) = \frac{1}{K} \sum_{k=1:K} |\mathbf{v}[k] - v(\mathbf{p}_k)|, \quad (5.8)$$

where  $v$  is the exact value of the flux, derived from the exact solutions, and  $\mathbf{v}[k]$  is the numerical result of flux at  $\mathbf{p}_k$ . Graph of the error function is shown in Figure 3 in field of  $s \in [0, 1]$  for  $N = 40$  and 80 when  $n = 8$  and 16. Note that, since the source points are selected symmetric on the boundary elements, the error function is also symmetric with respect to  $s$ , i.e.  $Er(s) = Er(-s)$  for  $s \in [0, 1]$ . According to Figure 3, error of linear BEM decreases significantly at  $s = \pm 0.58$  and  $\pm 0.43$  for  $n = 8$  and 16, respectively.

Example 5.1 shows the error of the linear BEM is minimized at some  $s$  which they are reported in Equation (5.3) as candidates for optimal points. Then from this investigation,

$$s = \begin{cases} \pm 0.58, & \text{if } n = 8, \\ \pm 0.43, & \text{if } n = 16, \end{cases} \quad (5.9)$$

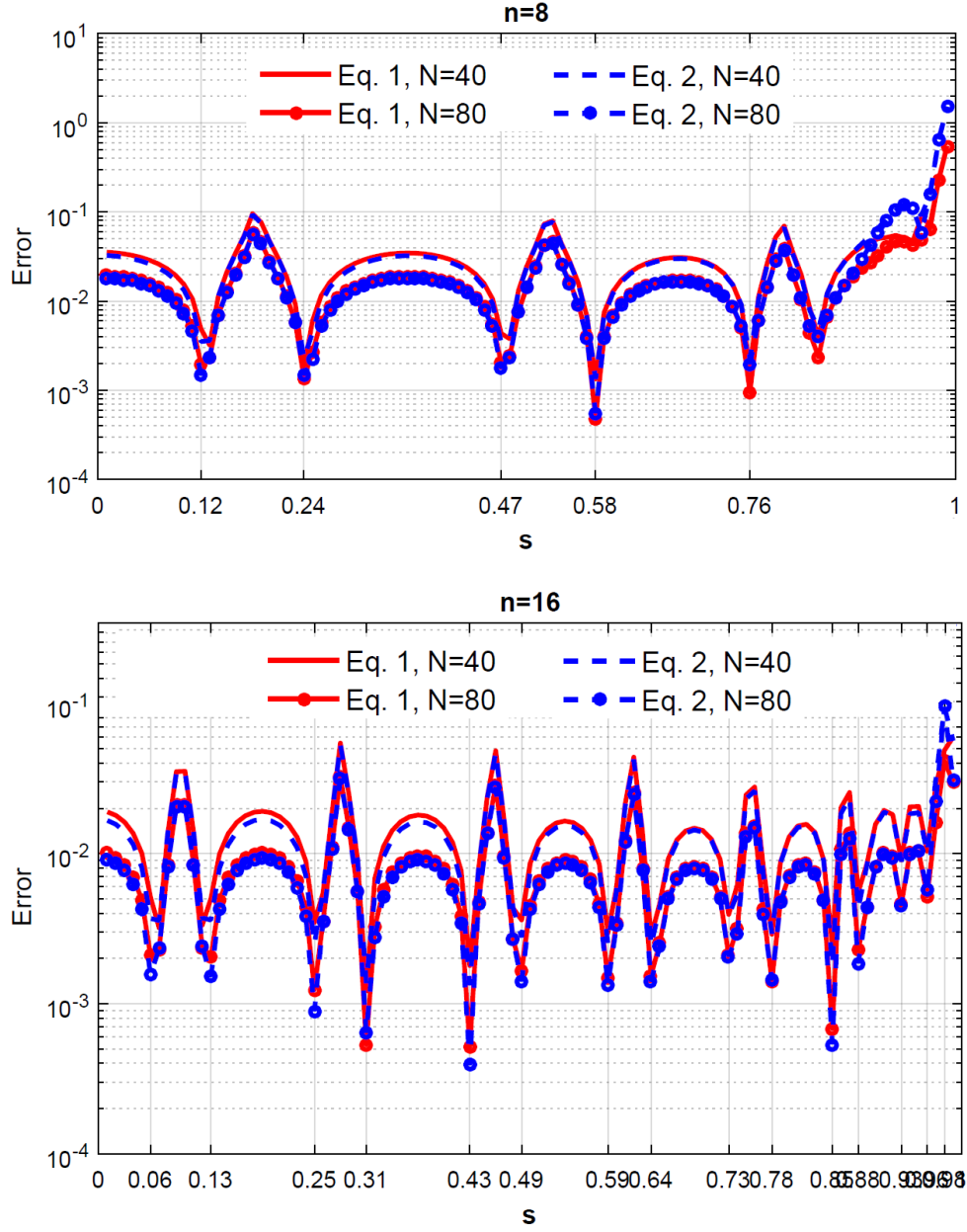


Figure 3: Graph of error of the linear BEM to solve Laplace equation in field of  $s$ . The boundary of domain is discretized to  $N = 40$  and  $80$  boundary elements for two exact solutions. It can be seen error of BEM reduces significantly when  $s = 0.12, 0.24, 0.47, 0.58, 0.76$  and  $s = 0.06, 0.13, 0.25, 0.31, 0.43, 0.49, 0.59, 0.64, 0.73, 0.78, 0.85, 0.88, 0.93, 0.96$  for  $n = 8$  (up) and  $n = 16$  (down), respectively.

may be appropriate candidate for  $s_{opt}$ . The example also show the optimal  $s$  depends on  $n$  but not on the solution when linear basis functions

$$\begin{aligned}\phi_{2j-1}(\mathbf{q}) &= -\frac{1}{2s}(t-s), \\ \phi_{2j}(\mathbf{q}) &= \frac{1}{2s}(t+s),\end{aligned}\tag{5.10}$$

are applied to approximate the unknown function on the boundary elements. Then Gaussian RBFs

$$\begin{aligned}\phi_{2j-1}(\mathbf{q}) &= \exp(-\epsilon^2 \|\mathbf{q} - \mathbf{p}_{2j-1}\|^2), \\ \phi_{2j}(\mathbf{q}) &= \exp(-\epsilon^2 \|\mathbf{q} - \mathbf{p}_{2j}\|^2),\end{aligned}\tag{5.11}$$

are applied in the next example to check the efficiency of proposed values (5.9) for RBFs. As is mentioned in Section 1, the Gaussian RBFs are stable and accurate if shape parameter  $\epsilon^2$  is selected optimally [25, 29]. It is well-known that smaller values of  $\epsilon^2$  leads more accurate but less stable results. Our experiment results show

$$\epsilon^2 = K^2/1000,\tag{5.12}$$

works well for the radial BEM when  $\Omega = [-1, 1]^2$ .

**Example 5.2.** *Let Laplace equation (5.5) is valid on  $\Omega = [-1, 1]^2$  with Dirichlet boundary condition. Then boundary of  $\Omega$  is divided to  $N$  boundary elements and the boundary functions are approximated by Gaussian RBFs (5.11) with shape parameter (5.12). The Laplace equation is solved for exact solutions (5.6) and (5.7) and the flux is obtained at boundary points (5.4) by the radial BEM. The error of the method is calculated by formulation (5.8) and is depicted in Figure 4 in field of  $s$  for  $N = 40$  and 80. Note that GQR with  $n = 8$  and 16 nodes are applied to calculate the boundary integrals. Figure 4 admits the error of the radial BEMs is minimized at that points reported in equation (5.9).*

Examples 5.1 and 5.2 show computational points (5.9) lead optimal results for linear and radial BEMs, respectively. Therefore we conclude

$$s_{opt} \simeq \begin{cases} \pm 0.58, & \text{if } n = 8, \\ \pm 0.43, & \text{if } n = 16, \end{cases}\tag{5.13}$$

are also optimal points for BEMs generated by the other basis functions. Note that although the optimal value of  $s$ , presented in Equation (5.13), is reported only for  $n = 8$  and 16, but the idea is also extensible for the other values of  $n$ . Numerical experiments show GQR is not sufficiently accurate for  $n \leq 8$  because semi-equality (4.8) is not valid for small values of  $n$ . The next numerical example show the rule is perfect when  $n = 16$  and there is no need to larger values of  $n$ .

**Example 5.3.** *linear BEM is applied in this example to solve Laplace equation (5.5) while its boundary integrals are calculated numerically and analytically. GQR with  $n = 16$  nodes is applied for numerical integration and the analytical technique presented in [12]*

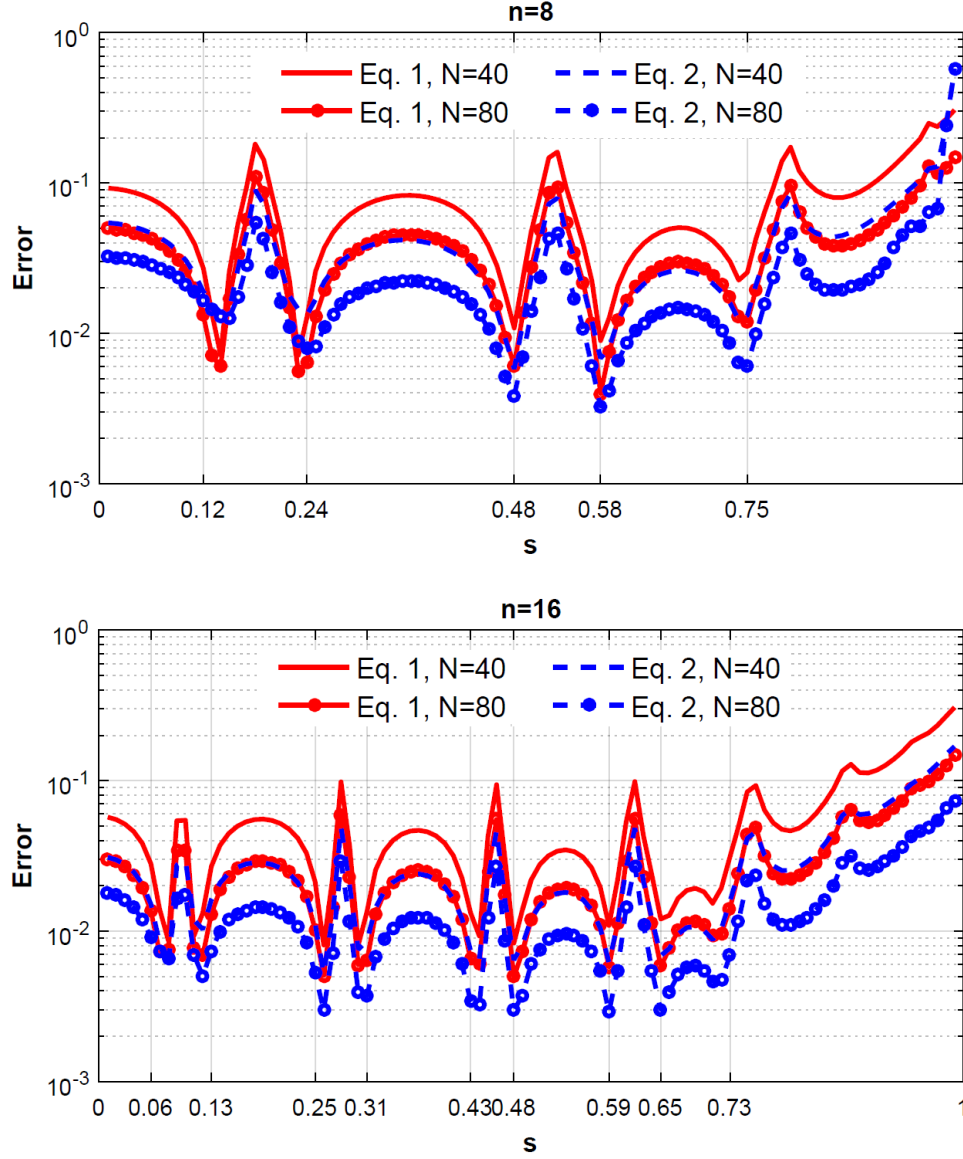


Figure 4: Graph of error of the radial BEM to solve Laplace equation in field of  $s$ . The boundary of domain is discretized to  $N = 40$  and 80 boundary elements for two exact solutions. It can be seen that error of the BEM reduces significantly when  $s = 0.12, 0.24, 0.47, 0.58, 0.75$  and  $s = 0.06, 0.13, 0.25, 0.31, 0.43, 0.49, 0.59, 0.64, 0.73$  when number of Gaussian quadrature points are  $n = 8$  (up) and  $n = 16$  (down), respectively.

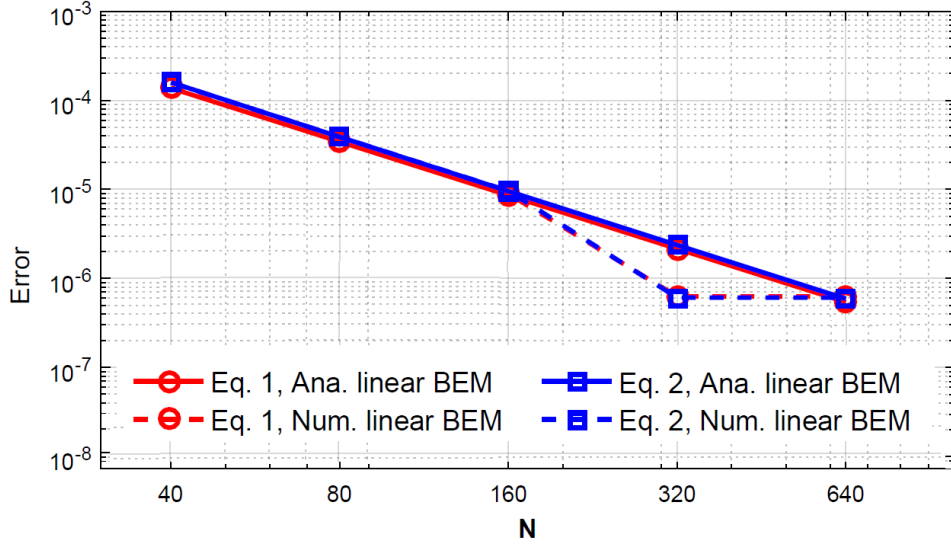


Figure 5: Graph of error of the linear BEM at some internal points. Boundary integrals are calculated analytically (Ana.) and numerically (Num.). Numerical integration is done by Gaussian quadrature rule with  $n = 16$  quadrature nodes. One can see the error of linear BEM when boundary integrals are calculated analytically is the same as the error when they are calculated numerically.

is applied for analytical integration. Computational domain is  $\Omega = [-1, 1]^2$  and Dirichlet boundary condition is imposed on boundary source points (5.4). Potential function is calculated numerically at internal points  $\hat{\mathbf{p}}_k = \frac{1}{2}\mathbf{p}_k$  for exact solutions (5.6) and (5.7). Error of the linear BEM is calculated as

$$Er = \frac{1}{K} \sum_{k=1:K} |\hat{u}_k - u(\hat{\mathbf{p}}_k)|, \quad (5.14)$$

where  $\hat{u}_k$  and  $u(\hat{\mathbf{p}}_k)$  are numerical and analytical values of the potential function at internal point  $\hat{\mathbf{p}}_k$ , respectively. The error of the method is demonstrated in Figure 5. From this figure, error of the linear BEM when its integrals are calculated numerically is the same as that when the integrals are obtained analytically. Then GQR is as accurate as the analytical technique when  $n = 16$ .

From Example 5.3, Gaussian quadrature rule with  $n = 16$  quadrature nodes is able to calculate boundary integrals of BEM, precisely. Note that analytical techniques are only applicable for polynomial basis functions defined on straight boundary elements [12, 8]. Then they are not applicable for RBFs defined on curved boundary elements. Consequently, the new technique, based on the GQR, enhances the ability of BEM, significantly. Since smooth RBFs have higher approximation power versus piecewise polynomials, radial BEM is significantly more accurate than the conventional BEM. In the next section some comparison tests are presented to verify this claim.



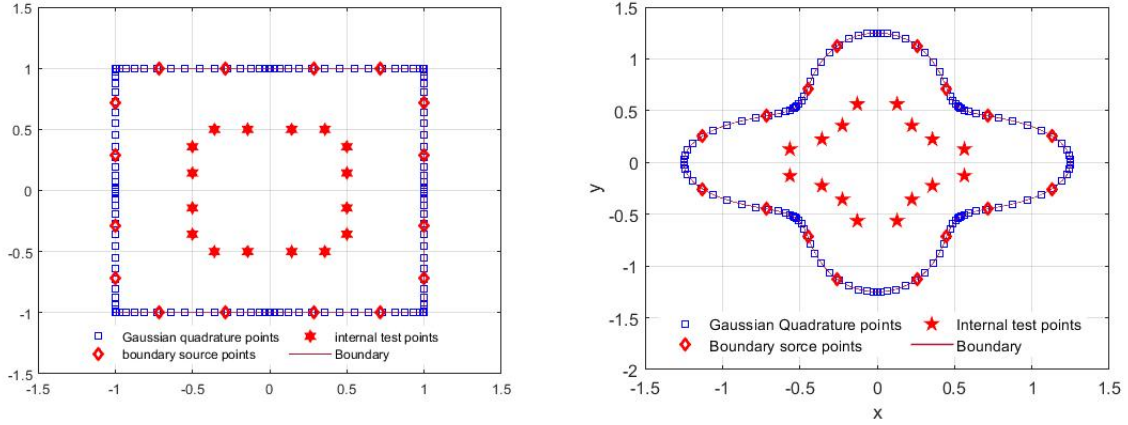


Figure 6: The square and flower-like domains. Boundary elements are straight and curved for the square and flower-like domains, respectively.

## 6 Numerical experiments

From Section 5, radial BEM is accurate when its boundary integrals are calculated by GQR with  $n = 16$  nodes. In this section, at first, the accuracy of radial BEM is studied for some well-known RBFs [28]. Then, accuracy of the radial BEM is compared with that of conventional BEM to solve some PDEs. The shape parameter of the RBFs is considered as (5.12) in this section. For numerical implementation, boundaries of computational domains are discretized to  $N$  semi-uniform boundary elements and  $K = 2N$  optimal boundary points are selected on them to approximate the boundary values as is described in Section 5.

### 6.1 Radial BEM for several RBFs

Let square domain  $\Omega = [-1, 1]^2$  is considered as computational domain and its boundary is discretized to  $N$  straight boundary elements. Figure 6 (left) shows the boundary when it is discretized to  $N = 8$  boundary elements and  $n = 16$  quadrature nodes are selected on each boundary element to calculate the boundary integrals. Then, two boundary source points correspond to optimal values (5.13) are selected on each boundary element. Consequently Laplace equation (5.5) is solved by Radial BEM and numerical error of the method is calculated by formulation (5.14) for internal points  $\hat{\mathbf{p}}_k = \frac{1}{2}\mathbf{p}_k$  for  $k = 1, 2, \dots, K$ . The error is reported in Table 2 for Gaussian, inverse multiquadric (IMQ), thin plate spline (TPS), poly-harmonic spline (PHS) and local  $C^0$  radial basis functions [28]. The first two RBFs are infinitely smooth functions containing shape parameter  $\epsilon^2$  is evaluated as (5.12). To study the accuracy of radial BEM, Dirichlet and mixed boundary conditions are imposed at the boundary source points by exact solution

$$u(x, y) = \exp(x) \cos(y).$$

In Dirichlet boundary condition potential is known at the boundary source points, while the potential value is available only at upper and lower sides of the square for the mixed boundary condition. The flux is available at left and right sides of the square for the mixed boundary condition. From Table 2, error of radial BEM is smaller than  $10^{-5}$  for Gaussian, IMQ, TPS and PHS RBFs when  $N \geq 64$  and Dirichlet boundary condition is imposed. Also the error is smaller than  $10^{-3}$  for the RBFs when  $N \geq 64$  and the mixed boundary condition is applied. Therefore radial BEM is accurate for the square domain. Then flower-like region

$$\Omega = \{(x, y) \in \mathbb{R}^2 \mid x = r \cos(\theta), y = r \sin(\theta), 0 \leq \theta \leq 2\pi, 0 \leq r \leq (1 + 0.25 \cos(4\theta))\},$$

is considered as an irregular domain to solve the problem by the radial BEM. Boundary of the domain is discretized to  $N$  curved boundary elements as is shown in Figure 6 (right) for  $N = 8$ . Similar to the square domain,  $K = 2N$  optimal boundary source points are selected on the boundary elements and boundary integrals are calculated by GQR with  $n = 16$  nodes. Error of the radial BEM is calculated by equation (5.14) for the RBFs and is reported in Table 3. From this table, the forth first RBFs yield sufficiently accurate results for  $N \geq 64$ .

Regarding tables 2 and 3, radial BEM is able to solve the BVP accurately when infinitely smooth RBFs are applied and the boundary integrals are calculated by GQR with  $n = 16$  nodes while the optimal boundary points are applied as source points.

Table 2: Numerical results of radial BEM for the square domain.

B.C.	RBF	$N$				
		8	16	32	64	128
Dirichlet	Gaussian	$7.84e-4$	$9.98e-5$	$1.91e-6$	$2.05e-6$	$2.15e-6$
	IMQ	$1.10e-3$	$1.78e-4$	$1.93e-5$	$8.27e-7$	$3.15e-7$
	TPS	$8.40e-3$	$1.91e-4$	$2.30e-5$	$3.11e-6$	$4.72e-7$
	PHS	$1.70e-3$	$9.57e-5$	$5.83e-6$	$1.06e-6$	$4.66e-7$
	Local $C^0$	$2.41e-2$	$8.60e-3$	$2.60e-3$	$7.14e-4$	$1.87e-4$
Mixed	Gaussian	$8.70e-3$	$2.10e-3$	$4.64e-4$	$3.01e-4$	$7.90e-5$
	IMQ	$9.10e-3$	$4.40e-3$	$1.70e-3$	$5.42e-4$	$1.66e-4$
	TPS	$1.44e-0$	$1.35e-2$	$2.30e-3$	$4.86e-4$	$1.12e-4$
	PHS	$2.54e-2$	$3.80e-3$	$8.27e-4$	$1.87e-4$	$4.43e-5$
	Local $C^0$	$4.37e-2$	$2.50e-2$	$1.09e-2$	$4.10e-3$	$1.40e-3$

## 6.2 Comparison of radial BEM with standard BEM

In this subsection accuracy of radial BEM is compared with accuracy of linear BEM to solve advection-diffusion equation

$$\nabla^2 u(x, y) + h_1 u_x(x, y) + h_2 u_y(x, y) + \lambda u(x, y) = 0, \quad (6.1)$$

Table 3: Numerical results of radial BEM for the flower-like domain.

B.C.	RBF	$N$				
		8	16	32	64	128
Dirichlet	Gaussian	$2.8e-3$	$9.0e-5$	$4.0e-6$	$1.5e-6$	$3.7e-6$
	IMQ	$2.7e-3$	$8.1e-5$	$5.0e-6$	$9.0e-7$	$2.9e-7$
	TPS	$2.1e-3$	$2.1e-4$	$2.7e-5$	$3.2e-6$	$3.5e-7$
	PHS	$3.1e-3$	$1.0e-4$	$1.5e-6$	$5.1e-7$	$2.2e-7$
	Local $C^0$	$3.3e-2$	$8.0e-3$	$2.0e-3$	$5.0e-4$	$1.2e-4$
Mixed	Gaussian	$2.1e-2$	$3.6e-3$	$2.2e-4$	$6.0e-6$	$1.6e-5$
	IMQ	$1.6e-2$	$2.8e-3$	$2.3e-4$	$1.4e-6$	$1.3e-6$
	TPS	$7.4e-2$	$2.3e-3$	$2.0e-4$	$2.3e-5$	$3.7e-6$
	PHS	$1.1e-2$	$7.3e-4$	$3.7e-5$	$2.1e-6$	$1.0e-6$
	Local $C^0$	$1.0e-1$	$5.5e-3$	$1.6e-3$	$4.0e-4$	$1.0e-4$

where  $h_1, h_2$  and  $\lambda$  are constant numbers. The square and flower-like regions are considered as computational domains where are shown in Figure 6. Boundary of the domains are discretized to  $N$  straight boundary elements in radial and linear BEMs. Then only approximation power of RBFs is compared by that of the linear polynomials when they are applied to approximate boundary values of BEM. The boundary integrals are calculated by GQR with  $n = 16$  nodes while the optimal boundary points are utilized. The Gaussian RBFs with shape parameter (5.12) are applied for the radial BEM, and Dirichlet boundary condition is imposed on the boundary of computational domains by exact solution

$$u(x, y) = \exp(x + y). \quad (6.2)$$

The mean value of error, Equation (5.14), is calculated for the methods at some internal points and is shown in Figure 7 when number of boundary elements are  $N = 40, 80, 120, 160$  and  $200$ . It can be found from the figure that the error of radial BEM is significantly less than the error of linear BEM which it shows higher approximation power of the RBFs versus polynomials.

## 7 Conclusion

To overcome the singularity problem of boundary elements method (BEM) this paper presented an efficient method for optimal selection of boundary source points. The new distribution of the source points allowed us to propose radial BEM. Then, radial BEM was described and its boundary integrals were calculated by Gaussian quadrature rule (GQR) with  $n = 16$  quadrature nodes, precisely. Radial BEM was studied numerically for several RBFs including Gaussian RBFs, and it was numerically compared with standard BEM via several examples. The results showed that radial BEM was much more accurate than standard BEM. The new method, applied to calculate the boundary integrals of

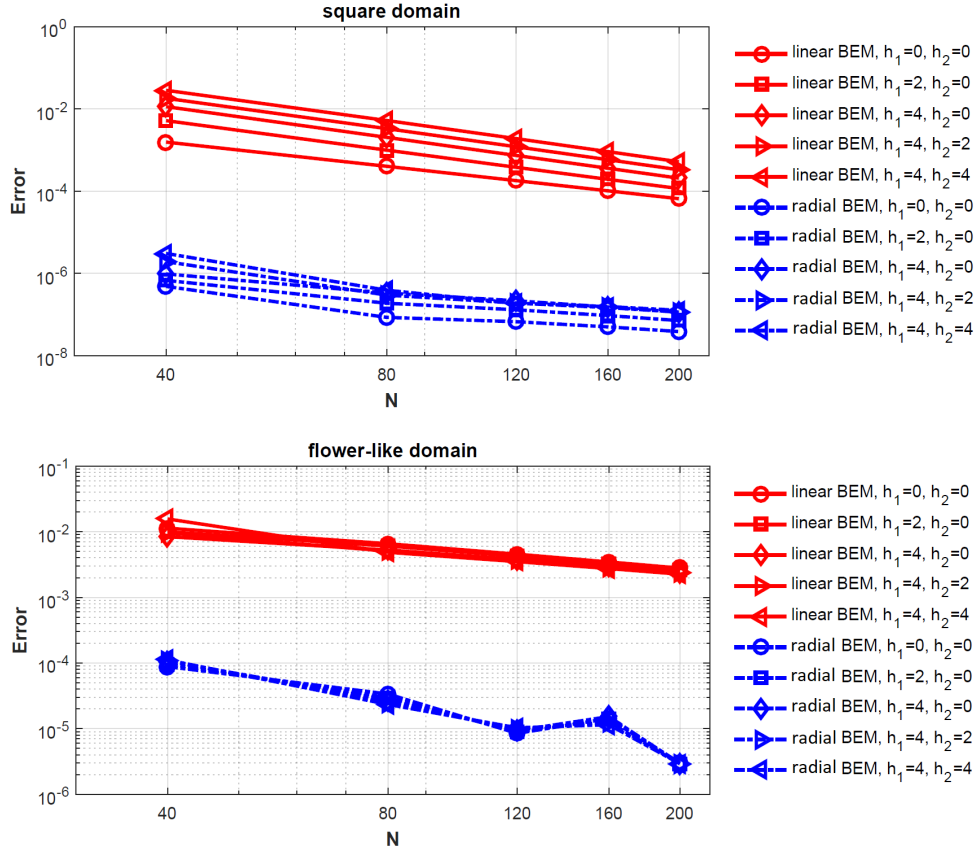


Figure 7: Graph of error of the linear and radial BEMs to solve advection-diffusion equation (6.1) for several  $h_1$  and  $h_2$  when computational domain is square (up) and flower-like (dawn). The boundary integrals are calculated by Gaussian quadrature rule with  $n = 16$  quadrature nodes. It is clear that the error of the radial BEM is significantly smaller than the error of the linear BEM in the all case studies.

BEM, also can be utilized for solving other boundary integral equations with singular kernels. Moreover, radial BEM can be extended to solve more complicated or three dimensional PDEs.

## References

- [1] C. A. Brebbia, The birth of the boundary element method from conception to application (2017).
- [2] Z. Sedaghatjoo, M. Dehghan, H. Hosseinzadeh, Numerical solution of 2d navier-stokes equation discretized via boundary elements method and finite difference approximation, *Engineering Analysis with Boundary Elements* 96 (2018) 64–77.
- [3] K. Li, T. Yang, W. Jiang, K. Zhao, K. Zhao, X. Xu, Isogeometric boundary element method for isotropic damage elastic mechanical problems, *Theoretical and Applied Fracture Mechanics* 124 (2023) 103802.
- [4] A. B. Sichani, C. Mehring, Boundary element method for modeling droplet deformation in secondary atomization, *Engineering Analysis with Boundary Elements* 152 (2023) 51–65.
- [5] H. Hosseinzadeh, M. Dehghan, D. Mirzaei, The boundary elements method for magneto-hydrodynamic (mhd) channel flows at high hartmann numbers, *Applied Mathematical Modelling* 37 (4) (2013) 2337–2351.
- [6] J. T. Katsikadelis, *Boundary Elements Theory and Applications*, Amsterdam: Elsevier, 2002.
- [7] M. Dehghan, H. Hosseinzadeh, Improvement of the accuracy in boundary element method based on high-order discretization, *Computers & Mathematics with Applications* 62 (12) (2011) 4461–4471.
- [8] M. Dehghan, H. Hosseinzadeh, Calculation of 2d singular and near singular integrals of boundary elements method based on the complex space  $c$ , *Applied Mathematical Modelling* 36 (2) (2012) 545–560.
- [9] H. Bin, N. Zhongrong, H. Zongjun, L. Cong, C. Changzheng, Boundary element analysis of the orthotropic potential problems in 2-d thin structures with the higher order elements, *Engineering Analysis with Boundary Elements* 118 (2020) 1–10.
- [10] P.-F. Hou, W.-H. Zhang, J.-p. Tang, J.-Y. Chen, Three-dimensional exact solutions of elastic transversely isotropic coated structures under conical contact, *Surface and Coatings Technology* 369 (2019) 280–310.

- [11] Z. Han, C. Cheng, Z. Hu, Z. Niu, The semi-analytical evaluation for nearly singular integrals in isogeometric elasticity boundary element method, *Engineering Analysis with Boundary Elements* 95 (2018) 286–296.
- [12] H. Hosseinzadeh, M. Dehghan, A simple and accurate scheme based on complex space  $c$  to calculate boundary integrals of 2d boundary elements method, *Computers & Mathematics with Applications* 68 (4) (2014) 531–542.
- [13] Q.-N. Yang, Y. Miao, An improved exponential transformation for accurate evaluation of nearly singular boundary integrals in 3d bem, *Engineering Analysis with Boundary Elements* 71 (2016) 27–33.
- [14] Y. Gu, H. Dong, H. Gao, W. Chen, Y. Zhang, An extended exponential transformation for evaluating nearly singular integrals in general anisotropic boundary element method, *Engineering Analysis with Boundary Elements* 65 (2016) 39–46.
- [15] Y. Miao, W. Li, J. Lv, X. Long, Distance transformation for the numerical evaluation of nearly singular integrals on triangular elements, *Engineering Analysis with Boundary Elements* 37 (10) (2013) 1311–1317.
- [16] F. Tan, J. Liang, Y. Jiao, S. Zhu, J. Lv, The bem based on conformal duffy-distance transformation for three-dimensional elasticity problems, *Science China Technological Sciences* (2020) 1–9.
- [17] Y. Gu, Q. Hua, W. Chen, C. Zhang, Numerical evaluation of nearly hyper-singular integrals in the boundary element analysis, *Computers & Structures* 167 (2016) 15–23.
- [18] Y. Gu, C. Zhang, W. Qu, J. Ding, Investigation on near-boundary solutions for three-dimensional elasticity problems by an advanced bem, *International Journal of Mechanical Sciences* 142 (2018) 269–275.
- [19] X.-W. Gao, J.-B. Zhang, B.-J. Zheng, C. Zhang, Element-subdivision method for evaluation of singular integrals over narrow strip boundary elements of super thin and slender structures, *Engineering Analysis with Boundary Elements* 66 (2016) 145–154.
- [20] J. Zhang, B. Chi, K. M. Singh, Y. Zhong, C. Ju, A binary-tree element subdivision method for evaluation of nearly singular domain integrals with continuous or discontinuous kernel, *Journal of Computational and Applied Mathematics* 362 (2019) 22–40.
- [21] P. Assari, F. Asadi-Mehregan, M. Dehghan, On the numerical solution of fredholm integral equations utilizing the local radial basis function method, *International Journal of Computer Mathematics* 96 (7) (2019) 1416–1443.

- [22] Y. Gu, H. Gao, W. Chen, H. Wang, C. Zhang, A general algorithm for evaluating nearly strong-singular (and beyond) integrals in three-dimensional boundary element analysis, *Computational Mechanics* 59 (5) (2017) 779–793.
- [23] Y. Gong, C. Dong, An isogeometric boundary element method using adaptive integral method for 3d potential problems, *Journal of Computational and Applied Mathematics* 319 (2017) 141–158.
- [24] L. Yuan, M. Wentao, W. Gangsheng, L. Jing, W. Shixun, A general-purpose machine learning framework for predicting singular integrals in boundary element method, *Engineering Analysis with Boundary Elements* 117 (2020) 41–56.
- [25] M. D. Buhmann, *Radial basis functions theory and implementations* (2017).
- [26] E. Tayari, L. Torkzadeh, D. Domiri Ganji, K. Nouri, Investigation of hybrid nanofluid swcnt–mwcnt with the collocation method based on radial basis functions, *The European Physical Journal Plus* 138 (1) (2023) 3.
- [27] N. Narimani, M. Dehghan, Predicting the effect of a combination drug therapy on the prostate tumor growth via an improvement of a direct radial basis function partition of unity technique for a diffuse-interface model, *Computers in Biology and Medicine* 157 (2023) 106708.
- [28] H. Wendland, *Scattered data approximation*, Vol. 17, Cambridge university press, 2004.
- [29] H. Wendland, *Scattered data approximation* (2010).
- [30] P. Assari, M. Dehghan, A meshless discrete collocation method for the numerical solution of singular-logarithmic boundary integral equations utilizing radial basis functions, *Applied Mathematics and Computation* 315 (2017) 424–444.
- [31] P. Assari, M. Dehghan, A meshless method for the numerical solution of nonlinear weakly singular integral equations using radial basis functions, *The European Physical Journal Plus* 132 (2017) 1–23.
- [32] P. Assari, M. Dehghan, The approximate solution of nonlinear volterra integral equations of the second kind using radial basis functions, *Applied Numerical Mathematics* 131 (2018) 140–157.
- [33] P. Assari, M. Dehghan, The numerical solution of two-dimensional logarithmic integral equations on normal domains using radial basis functions with polynomial precision, *Engineering with Computers* 33 (4) (2017) 853–870.
- [34] R. L. Hardy, Multiquadric equations of topography and other irregular surfaces, *Journal of geophysical research* 76 (8) (1971) 1905–1915.

- [35] M. Mongillo, et al., Choosing basis functions and shape parameters for radial basis function methods, SIAM undergraduate research online 4 (190-209) (2011) 2–6.
- [36] C.-S. Chen, A. Noorizadegan, D. Young, C. Chen, On the selection of a better radial basis function and its shape parameter in interpolation problems, Applied Mathematics and Computation 442 (2023) 127713.
- [37] G. E. Fasshauer, Meshfree approximation methods with MATLAB, Vol. 6, World Scientific, 2007.
- [38] N. Ortner, P. Wagner, Fundamental solutions of linear partial differential operators, Springer, 2015.
- [39] H. Hosseinzadeh, M. Dehghan, Z. Sedaghatjoo, The stability study of numerical solution of fredholm integral equations of the first kind with emphasis on its application in boundary elements method, Applied Numerical Mathematics (2020).
- [40] D. N. Arnold, A concise introduction to numerical analysis (1991).